MANCHESTER 1824
The University of Manchester

The University of Manchester Research

Synthesis, X-ray single-crystal structural characterization and thermal analysis of bis(O-alkylxanthato)Cd(II) and bis(O-alkylxanthato)Zn(II) complexes used as precursors for cadmium and zinc sulfide thin films

DOI:
10.1021/acs.inorgchem.1c01110

Document Version
Accepted author manuscript

Link to publication record in Manchester Research Explorer

Citation for published version (APA):
Bakly, A., Collison, D., Ahumada Lazo, R., Binks, D., Smith, M., Raftery, J., Whitehead, G. F. S., O'Brien, P., & Lewis, D. (2021). Synthesis, X-ray single-crystal structural characterization and thermal analysis of bis(O-alkylxanthato)Cd(II) and bis(O-alkylxanthato)Zn(II) complexes used as precursors for cadmium and zinc sulfide thin films. *Inorganic Chemistry*, *60*(10), Article 7573–7583. https://doi.org/10.1021/acs.inorgchem.1c01110

Published in:
Inorganic Chemistry

Citing this paper
Please note that where the full-text provided on Manchester Research Explorer is the Author Accepted Manuscript or Proof version this may differ from the final Published version. If citing, it is advised that you check and use the publisher's definitive version.

General rights
Copyright and moral rights for the publications made accessible in the Research Explorer are retained by the authors and/or other copyright owners and it is a condition of accessing publications that users recognise and abide by the legal requirements associated with these rights.

Takedown policy
If you believe that this document breaches copyright please refer to the University of Manchester's Takedown Procedures [http://man.ac.uk/04Y6Bo] or contact openresearch@manchester.ac.uk providing relevant details, so we can investigate your claim.

OPEN ACCESS

Download date:17. Apr. 2025

Synthesis, X-ray single-crystal structural characterization and thermal analysis of bis(O-alkylxanthato)Cd(II) and bis(O-alkylxanthato)Zn(II) complexes used as precursors for cadmium and zinc sulfide thin films

Ali A.K. Bakly[a], David Collison[b], Ruben Ahumada-Lazo[c] David J. Binks[c], Matthew Smith[a], James Raftery[b], George F. S. Whitehead[b], Paul O'Brien,[a,b] and David J. Lewis.[a]*

Abstract

This work investigates tuning of the molecular structure of a series of O-alkylxanthato zinc and cadmium precursor complexes to enhance production of ZnS and CdS materials used in solar cells. Single crystals of bis(O-alkylxanthato) cadmium(II) complexes (**8–13**) and bis(O-alkyl xanthato)zinc(II) complexes (**18** and **19**) are reported. CdS and ZnS films were produced by the spin coating of these molecular precursors followed by thermal decomposition.Thin films of CdS were deposited by spin coating the bis(O-alkylxanthato) cadmium(II), precursors (**7–13**) on glass substrates, followed by annealing up to 300 °C for 60 min. The films of ZnS were deposited by spin coating bis(O-alkylxanthato) zinc(II), complexes (**14–20**), followed by annealing up to 200 °C for 60 min. The molecular complexes and solid state materials are characterised using a range of techniques including single-crystal X-ray diffraction, pXRD, EDS and XPS, DSC and TGA, UV-Vis and PL spectroscopies and electron microscopy. These techniques provided information on the influence of alkyl chain length on the thermal conditions required to fabricate metal sulfide films as well as film properties such as relative numbers of defect sites, films quality and morphology, for example, the obtained crystallite size of metal sulfide films formed is correlated to the hydrocarbon chain length of the precursor. The behaviour of the complexes under thermal stress was studied. DTA and TGA profiles explain the relationship between hydrocarbon chain length, decomposition temperatures and the energies required for decomposition. A higher decomposition temperature for complexes with longer hydrocarbon chains is observed compared to complexes with shorter hydrocarbon chains. Band-gap energies calculated from the optical absorption spectra alongside steady state and time resolved photoluminescence studies are reported for CdS films.

Introduction

Alkylxanthato cadmium and zinc complexes have been used as single source molecular precursors towards thin films of cadmium sulfide (CdS) and zinc sulfide (ZnS) respectively.[1–7] CdS is a II−VI compound semiconductor with a wide direct band-gap (2.4 eV), making it useful in a variety of electronic and photovoltaic applications.[8] CdS crystallizes in hexagonal (wurtzite) and cubic (zinc blende) structures. Ramasamy et al.,[2] have reported that CdS film growth, depends on the influence of precursors, methods and synthetic conditions. The successful synthesis of face-centered cubic CdS nanoparticles was reported by Wang and co-authors,[9] through a synthetic process of liquid-solid-solution phase transfer and separation. ZnS is another II-VI semiconductor with an even wider direct band-gap of 3.7 eV.[1] ZnS exists as hexagonal wurtzite or cubic zinc blende polymprphs. Ma et al., described wurtzite ZnS as composed of alternating planes of tetrahedrally coordinated S^{2-} and Zn^{2+} ions, stacked along the *c*-axis. [10] Moore et al, showed that phase transformation between zinc blende and wurtzite occurs through changes in stacking sequence.[11]

Precursors of Cd^{2+} and Zn^{2+} with xanthate ligands are typified by the formation of weak polymeric structures in solution. A monoclinic crystal structure of bis(methoxyethyl-xanthato)cadmium, $Cd(S_2COCH_2CH_2OCH_3)_2$, which is a metal xanthate precursor toward CdS materials formation, for example, has been determined by Abrahams et al.[12] Such complexes have several unique features by which to act as precursors for thin film deposition of metal sulfides including a pre-formed network of metal-sulfur bonds, which enables low temperature decomposition to the corresponding metal sulfide, which is relatively clean due to the generation of gaseous side products. Bakly et al.,[1] have been demonstrated a new way to produce CdS, ZnS and CdZnS thin films by an inexpensive synthetic technique based on spin-coat and annealing. Thomas et al.,[13] reported high quality nano-crystalline thin films of CdS, ZnS, CuS and PbS nanoparticles from thiobiuret complexes $[M(SON(CN^iPr_2)_2)_2]$ as a single source precursor. Lewis et al.,[14] have reviewed the synthesis by melts of precursors and concluded that self-capping reactions are exceedingly simple and potentially scalable for nanoparticle synthesis. Afzaal et al.,[15] reported synthetic method from single molecule precursors of binary chalcogenides of the first transition series together of zinc or cadmium. Ramasamy et al.,[16] reviewed developments in synthetic routes to materials that have applications in solar cells: emerging materials such as bismuth sulfide, ternary materials such as copper indium sulfide, and copper zinc tin sulfide as quaternary material.

Metal chalcogenide compounds with thiolate ligands may possess polymeric structures in solution and the solid state and can be rendered involatile. The lack of volatility in general means these chalcogenide compounds are not useful as precursors for thin film deposition techniques such as LP-MOCVD.[15,17] Single source molecular precursors of precisely defined composition can provide a high degree of control during nanocrystal synthesis. Many studies have demonstrated the growth of binary and ternary nanostructures of transition metal chalcogenides as thin films, nanocrystals, nanosheets, nanoplates, nanowires, nanoribbons and others for energy applications.[14,18–20]

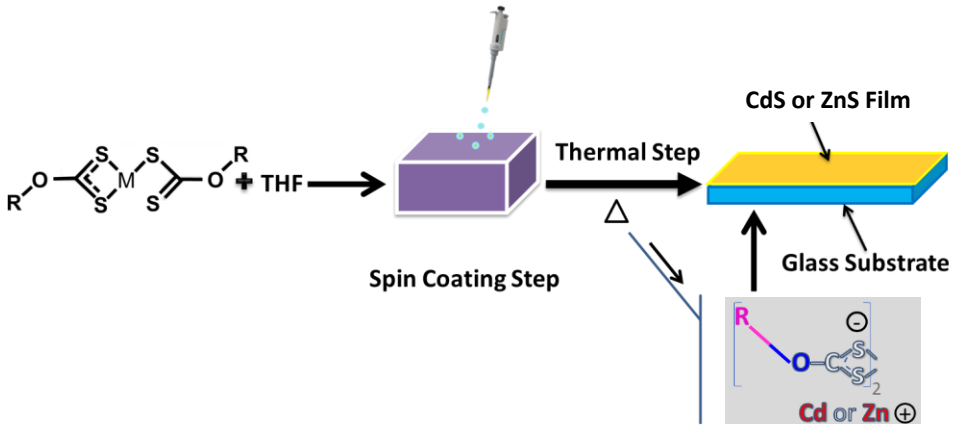

Figure 1 The schematic process of the formation of metal sulfide films from bis(O-alkylxanthato)cadmium(II) or zinc(II) compounds by spin-coating.

In this study, a series of metal-xanthato precursors (**7**–**20**) were synthesized. The work is grouped into three main sections; an X-ray crystallographic study of precursor structure, thermal analyses of precursors, and film deposition using spin-coating methods and subsequent structural and optical characterization of the resulting solid state materials New single crystals of metal alkylxanthato precursors are presented, which display the involved elements and their connectivity to metal centres. We also focus on the decomposition conditions and the thermal behavior of the metal xanthate complexes. We find that the ligand structure plays a role in the energy required for thermal decomposition of metal alkylxanthato precursors. Figure 1 displays a schematic process of formation inorganic films of ZnS and CdS by thermal decomposition of the corresponding zinc and cadmium alkylxanthato precursors. The films were prepared by spin coating of the metal xanthate complexes followed by annealing at relatively low temperatures in a nitrogen atmosphere.

The study we present demonstrates that the structure of the ligand is the predominant factor in controlling the decomposition of metal xanthate complexes.

Experimental section

Solvents and Reagents

Potassium hydroxide (≥85%), ^{n}propanol (≥99%), carbon disulfide (≥98.99%), petroleum ether (≥98.99%), hexane (≥97%), acetone (≥99%), ^{n}butanol (≥99%), ^{n}pentanol (≥99%), ^{n}hexanol (≥98%), ^{n}heptanol (≥98%), ^{n}octanol (≥99%), potassium ethylxanthate (≥98%), cadmium chloride (≥99%), zinc chloride (≥97%), acetonitrile (≥99.99%), methanol (≥99.8%), ethyl acetate (≥99.5%), tetrahydrofuran (≥99.99%) and N-methyl-2-pyrrolidone (≥99. %) were purchased from Sigma-Aldrich or Fisher and used without further purification. Deuterated solvents for NMR were purchased from Sigma-Aldrich.

Materials characterisation

Elemental analysis was conducted in the micro-analytical laboratory at the University of Manchester with a Carlo Erba EA 1108 / Flash 2000 Thermo Scientific elemental analyser. Thermogravimetric Analysis (TGA) and Differential Scanning Calorimetry (DSC) were recorded from 30 °C to 600 °C at 10 °C min^{-1} heating rate under dinitrogen N_2, using a Mettler Toledo TGA-DSC1 stare. Fourier transform infrared (FTIR) spectra were obtained using a Nicolet iS5 IR Spectrometer-Thermo Fisher Scientific, ESI; Figure S21 and S1.22. Nuclear magnetic resonance (NMR) spectra were recorded using a 400 MHz Bruker instrument, see Figure S1–S20. Melting point measurements were carried out in a capillary tube using a Stuart-melting point SMP10 device. Powder X-ray diffraction 'p-XRD' measurements were carried out at room temperature by using a Bruker D8 Advance diffractometer, using Cu-Kα radiation, (1.5418 Å), 40 kV, 40 mA. The scanning range was between 20° and 80° with a step size of 0.050˚ and a dwell time of 8 s. The diffraction patterns were processed using X'Pert High Score Plus software. High resolution transmission electron microscopy (HRTEM) images and energy dispersive X-ray spectroscopy (EDS) spectra were obtained using an FEI Talos F200A microscope equipped with X-FEG electron source and Super-X SDD EDS detectors. The experiment was performed using an acceleration voltage of 200 kV and a beam current of approximately 1 nA. TEM images were recorded with an FEI CETA 4K CMOS camera. STEM images were acquired with a high angle annular dark field (HAADF) detector. Photoluminescence (PL) decays were recorded using a Time-Correlated Single-Photon Counting (TCSPC) system, equipped with a mode-locked Ti:

sapphire laser (Spectra Physics Mai-Tai HP). The photoluminescence from the samples was collected and focused into a monochromator (Spex 1870c). Emission was detected using a multi-channel detector (Hamamatsu R3809U-50). The time correlation of detected photons was performed with the use of a PC electronic card from Edinburgh Instruments (TCC900). Absorption spectra were recorded with a Shimadzu double beam spectrophotometer, model UV-1800, wavelength range between 800–300 nm at 1 nm resolution. Single crystal X-ray diffraction data for the compounds were collected on a dual source Rigaku FR-X rotating anode diffractometer, using a Mo-Kα wavelength at 150 K, and reduced using CrysAlisPro 171.39.21a. The structures were solved and refined using Shelx-2016 implemented through Olex2 v1.2.8. CIF files were deposited with the CCDC, 1812163 (**8**), 1812158 (**9**), 1812159 (**10**), 1812157 (**11**), 1812160 (**12**), 1812156 (**13**), 1812161 (**18**), 1812162 (**19**).

Synthesis of molecular precursors

Fourteen different metal xanthato compounds, precursors (**7–20**) be described in this section, with the structures **8–13**, **18** and **19** being demonstrated as new single crystals. All syntheses of the ligand substituents (**1–6**) and precursors (**7–20**) were performed under dry dinitrogen N_2, using standard Schlenk techniques. The ligands substituents (**1–6**) and precursors (**7–20**) were prepared as described in the literature.[1,21] The tuning of surface morphology of thin film nanostructures is an essential step in optimization of solar cell layers and has a strong influence on the optical properties of the films.[1] Toward this end, the impact precursor structure has on the film microstructure/nanostructures has been widely reported.[22–24] The synthetic methods, elemental analysis, NMR data and other characterization of ligands and precursors are fully described in ESI.

Results and discussion

Seven bis(O-alkylxanthato)cadmium(II), [Cd($S_2COR)_2$] precursors: [Cd($S_2COEt)_2$] (**7**), [Cd($S_2CO^nPr)_2$] (**8**), [Cd($S_2CO^nBu)_2$] (**9**), [Cd($S_2CO^nPen)_2$] (**10**), [Cd($S_2CO^nHex)_2$] (**11**), [Cd($S_2CO^nHep)_2$] (**12**) and [Cd($S_2CO^nOct)_2$] (**13**) were synthesised by metathesis of cadmium(II) salts in water. Bis(O-alkylxanthato)zinc(II) precursors: [Zn($S_2COEt)_2$] (**14**), [Zn($S_2CO^nPr)_2$] (**15**), [Zn($S_2CO^nBu)_2$] (**16**), [Zn($S_2CO^nPen)_2$] (**17**), [Zn($S_2CO^nHex)_2$] (**18**), [Zn($S_2CO^nHep)_2$] (**19**) and [Zn($S_2CO^nOct)_2$] (**20**) were synthesised by metathesis of zinc(II) salts in water. All precursors (**7**–**20**) were soluble in the common organic solvents, *e.g.* THF or acetonitrile.

Single crystal X-ray structures of Cd and Zn Xanthates

Single crystals of precursors **8–13**, **15**, **18** and **19** of suitable quality for X-ray diffraction were grown by evaporation from acetonitrile. Compounds **8–11** and **13** crystallized in the monoclinic crystal system and compound **12** crystallized in the orthorhombic system. The molecular structures of [Cd($S_2CO^nPr)_2$] (**8**), [Cd($S_2CO^nBu)_2$] (**9**), [Cd($S_2CO^nPen)_2$] (**10**), [Cd($S_2CO^nHex)_2$] (**11**), [Cd($S_2CO^nHep)_2$] (**12**) and [Cd($S_2CO^nOct)_2$] (**13**) are shown in Figure 2(a–f). In all cases the cadmium ion is coordinated with four sulfur atoms with four bridging xanthate ligands to form a network, with each sulfur atom spanning across two adjacent cadmium atoms to form a distorted tetrahedral environment at the metal centre. The coordination environment at Cd centres with other bonds omitted for clarity is shown in ESI Figure S25. The refinement data of crystals for compounds **8–13** are presented in Table S1.

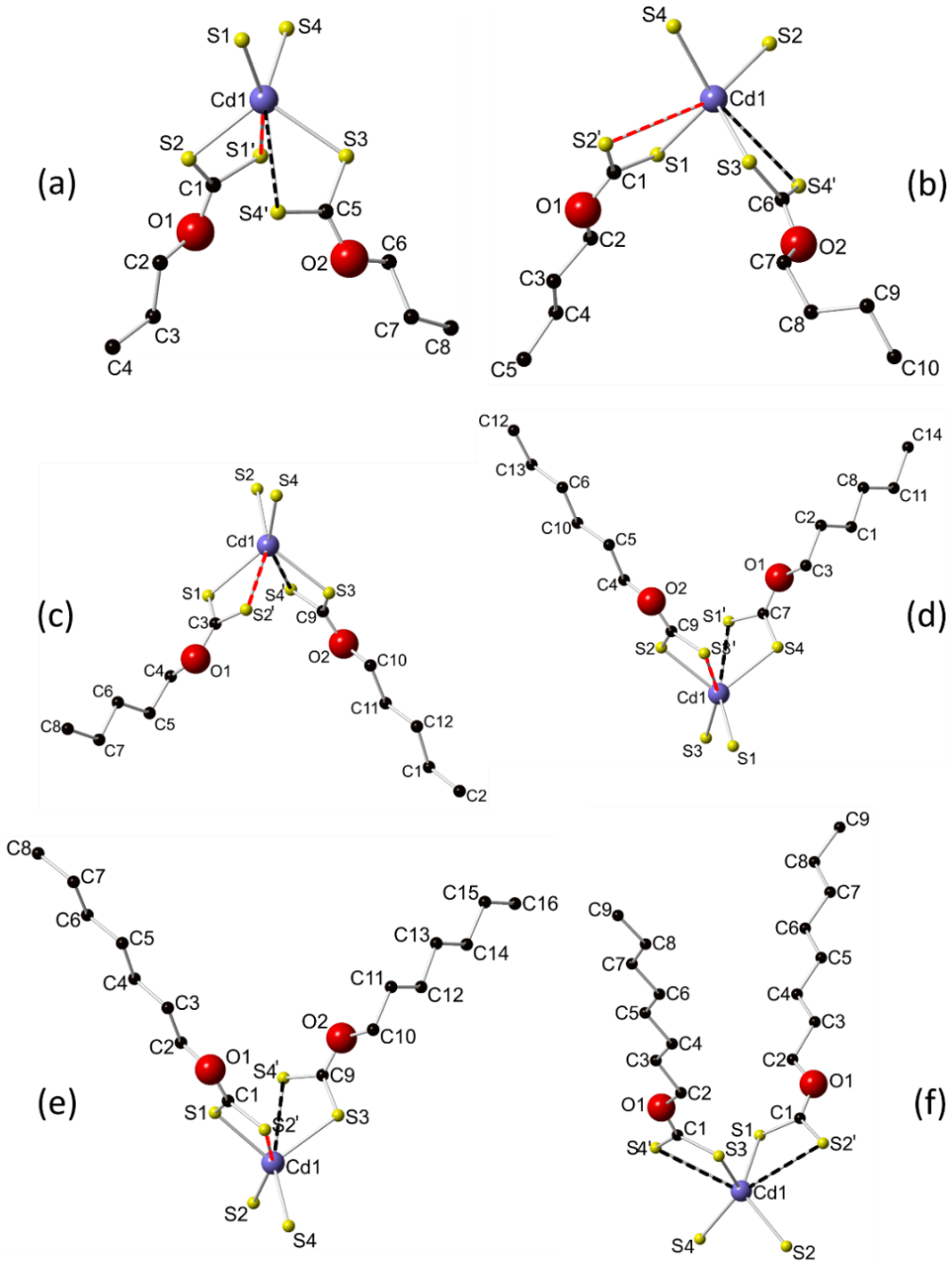

Figure 2 Single crystal X-ray structures of alkylxanthato cadmium(II) compounds **8–13** (a) $[Cd(S_2CO^nPr)_2]$, (b) $[Cd(S_2CO^nBu)_2]$, (c) $[Cd(S_2CO^nPen)_2]$, (d) $[Cd(S_2CO^nHex)_2]$, (e) $[Cd(S_2CO^nHep)_2]$ and (f) $[Cd(S_2CO^nOct)_2]$. The longer Cd-S bonds in the ligand (a-e) are represented as black and red dashed lines while the longer Cd-S bonds in (f) are equivalent and appear as black dashed lines. Structures were deposited as CCDC numbers, 1812163 (**8**), 1812158 (**9**), 1812159 (**10**), 1812157 (**11**), 1812160 (**12**), 1812156 (**13**).

The structure [Cd($S_2CO^nPen)_2$] (**10**) shows Cd in a distorted tetrahedral geometry, with additional electrostatic interactions with non-coordinating oxygen and sulfur from nearest neighbor xanthates. The four different coordinating S have Cd-S bond distances in the range of 2.5373(9) to 2.5764(8) Å, with S-Cd-S angles ranging between 101.49(3) and 122.95(3)°. There are two additional sulfur atoms and one additional oxygen close to the cadmium centres at 3.3531(8), 3.3801(8) and 3.016(2), respectively. These are at the limits of the sum of van der Waals radii for Cd and S (3.38 Å,) and Cd and O (3.1Å), respectively[25], see Figure 3 (b). These additional interactions are likely a consequence of the imperfect tetrahedral geometry around the Cd metal,[12] which leads to asymmetric arrangements of xanthate ligands in the structures.[26] The bonds lengths and angles found in the X-ray structures of compounds (**8-13**) are compiled in the ESI Table S2. There a number of reports of similar coordination of sulfur atoms in bis(ethylxanthato)cadmium(II) complexes where sulfur bridges two adjacent cadmium atoms in two different directions forming a two-dimensional network.[27-30] To reflect this we compiled the differences in Cd-S bonds lengths correlated with number of carbons in the xanthate ligands for (**8–13**) and (**15**, **18** and **19**) (Figure S23). Similarly, the correlation between unit cell volume with the carbon chain length of the xanthate ligand for (**8–13**) is shown in Figure S24.

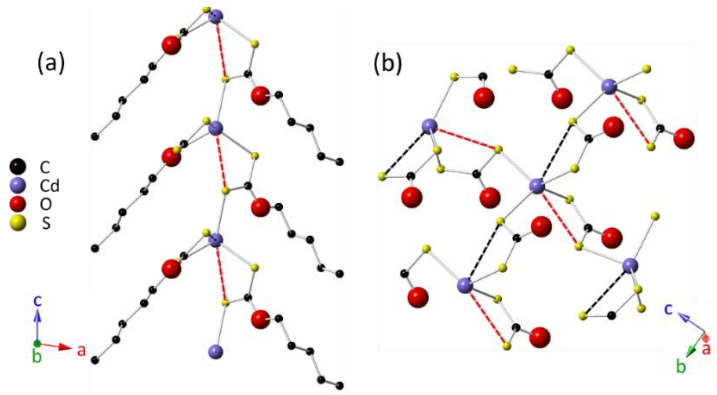

Figure 3 Views of the intermolecular packing in a single crystal of [Cd($S_2CO^nPen)_2$], (**10**), showing (a) the polymeric structure, (b) 4+2 coordination at the Cd centre. Black and red dashed lines correspond to the longer bonds of 3.374 Å and 3.354 Å, respectively. CCDC number 1812159.

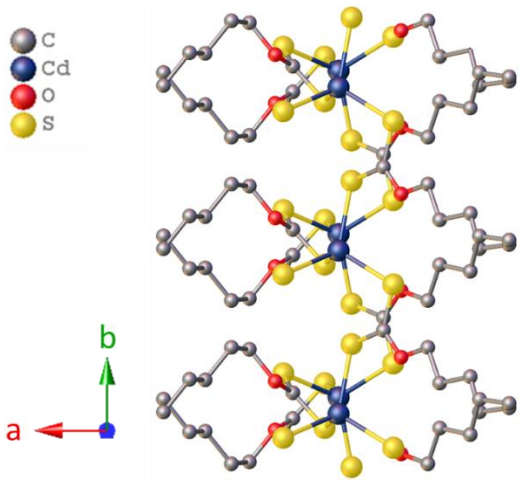

Figure 4 Intermolecular packing in single crystals of [Cd($S_2CO^nPen)_2$], (**10**). The view is projected along the *c* axis of the unit cell.

The structure of [Zn($S_2CO^nPr)_2$] (**15**) previously reported by Lai et al[31] can be compared to [Zn($S_2CO^nHex)_2$] (**18**) and [Zn($S_2CO^nHep)_2$] (**19**) and all are shown in Figure 5 (a–c). Compounds **18** and **19** crystallize in the monoclinic crystal system with space-group Cc. In both cases, the zinc ion is coordinated by four monodentate ligands, with a single ligand bridging across two zinc ions in a distorted tetrahedral environment forming a network similar to that which we observe with the Cd xanthates we report. The asymmetric unit of **15** has a 16-membered ring structure as described by Ito et al[32] (Figure S28 and Table S4). The molecular packing in crystals of **19**, is shown in Figure 6a,b. The coordination environments of the distorted tetrahedron at Zn centres with other bonds omitted for clarity are shown in Figure S27. The data from the X-ray analysis of Zn xanthates is compiled in Table S3. Bond lengths and angles for complexes **15**, **18** and **19** are reported in Table S4.

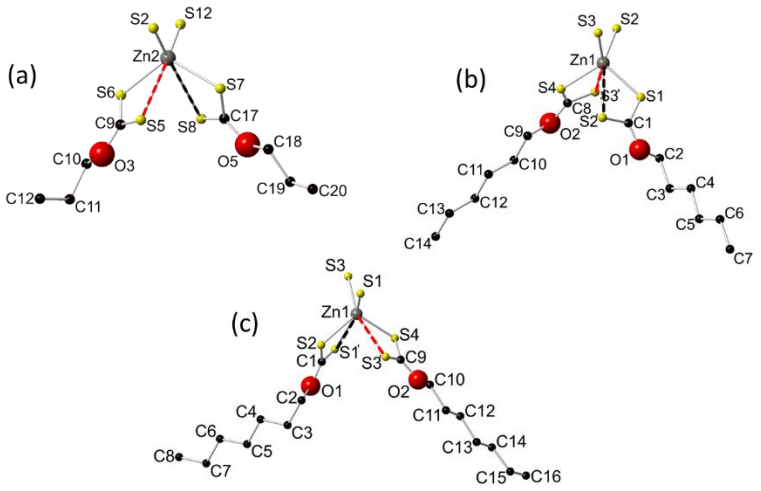

Figure 5 Crystal structures of alkylxanthato zinc complexes. (a) $[Zn(S_2CO^nPr)_2]$ as reported by Lai et al [31] (**15**), (b) $[Zn(S_2CO^nHex)_2]$ (**18**) and (c) $[Zn(S_2CO^nHep)_2]$ (**19**). The longer bonds of the ligand are represented as a black and a red dashed line. Hydrogen atoms are omitted for clarity. Structures of **18** and **19** were deposited as CCDC 1812161 and 1812162. The data for structure **15** is published in Ref 31 and is re-used with permission from The Royal Society of Chemistry.

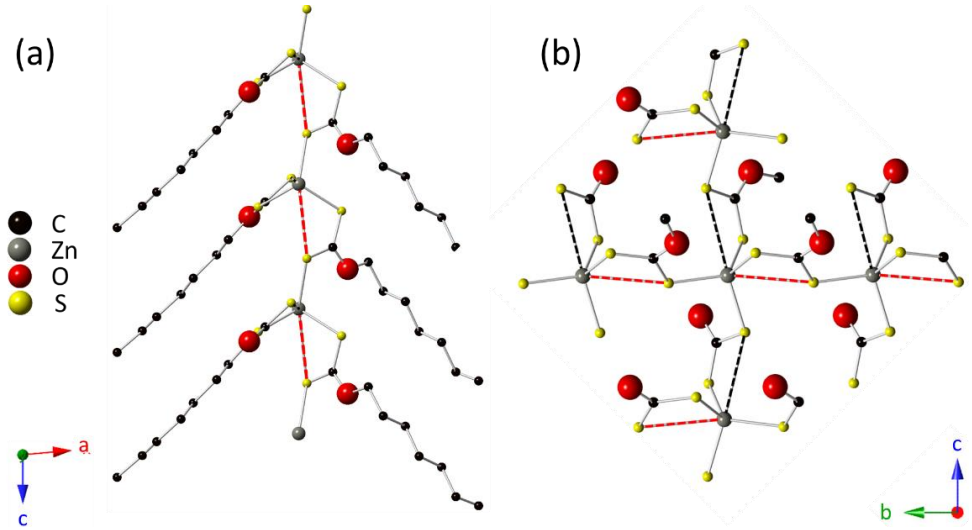

Figure 6 Intermolecular packing in single crystals of $[Zn(S_2CO^nHep)_2]$ (**19**) showing (a) packing that forms a polymeric structure and (b) coordination at Zn projected along the *a* axis of the unit cell. The longer Zn-S bonds are represented as a black and a red dashed line of 3.459 Å and 3.342 Å, respectively.

Thermal analysis of Cd and Zn Xanthates

It has been reported that xanthate ligands with longer hydrocarbon chains have a weaker affinity for the metal ion in metal xanthate complexes,[33] and hence it may be expected that there will be differences in the thermal profiles for each complex, and we investigated this phenomenon in detail for our Zn and Cd complexes. Thermogravimetric analysis (TGA) and differential scanning calorimetry (DSC) of the complexes was performed up to 600 °C under a nitrogen atmosphere in all cases, and from this we generate data on decomposition pathway and the energy required for each step. By the use of the series of complexes with increasing alkyl chain length we were able to infer the effect of ligand structure on the nature of the decomposition reactions for these complexes.

The TGA profile complexes **7**–**13** are shown in Figure 7. The mass-loss for these complexes occurs in general through two steps with a rapid mass loss within the temperature range of 145 to 170 °C and gradual mass loss between 175 to 300 °C. The mass-loss for complexes **10**–**13** occurs through three steps found at approximately 135 °C, 162 °C and 262–300 °C, respectively. The measured mass-loss of CdS corresponds to the calculated value of precursors **7-13** as following, (measured: calculated) %; (41.30: 40.74), (39.9: 37.75), (38.9: 35.17), (36.0: 32.92), (34.9: 30.94), (33.0: 29.18), (33.5: 27.62). Table S5 presents the compiled data for onset temperature, the experimental and theoretical residual mass, the melting points and some melting points in literature for bis(O-alkylxanthato)cadmium(II) precursors (**7–13**). MacLachlan et al.,[21] have described similar profiles for Cd xanthate complexes with pyridine adducts, but these also additional mass loss steps corresponding to the loss of the pyridine adducts. We note in some cases that above 200 °C that there is some additional mass loss which could potentially correspond to the loss of sulfur by sublimation.

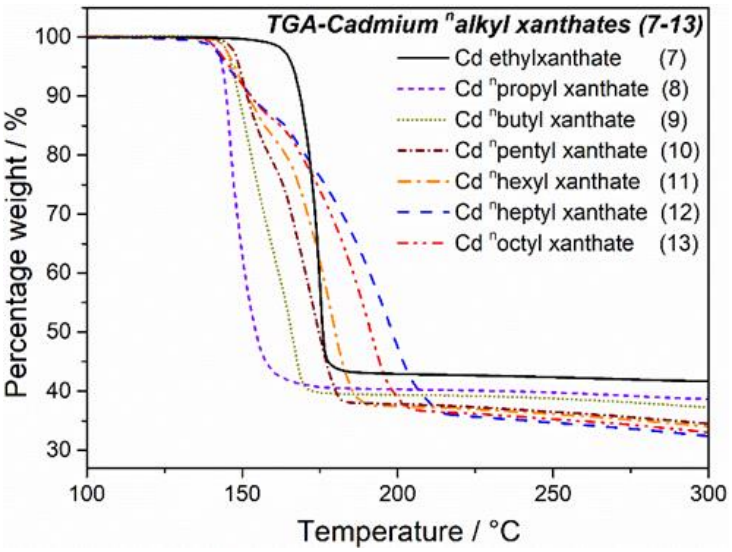

Figure 7 Thermogravimetric analysis TGA profiles of bis(O-alkylxanthato)cadmium(II), compounds **7**–**13**; heated in the range 100 – 300 °C with a temperature gradient of 10.0 °C min^{-1}.

Figure 8 shows TGA profiles for bis(O-alkylxanthato)zinc(II), compounds (**14–20**): $[Zn(S_2CO^nEt)_2]$ (**14**), $[Zn(S_2CO^nPr)_2]$ (**15**), $[Zn(S_2CO^nBu)_2]$ (**16**), $[Zn(S_2CO^nPen)_2]$ (**17**), $[Zn(S_2CO^nHex)_2]$ (**18**), $[Zn(S_2CO^nHep)_2]$ (**19**) or $[Zn(S_2CO^nOct)_2]$ (**20**), in the range 30–600 °C. The initial decomposition temperature of the compounds **14–20** were 144.7, 137.2, 137.7, 137.8, 138.7, 137.0, and 137.0 °C, respectively. The mass loss of the compounds with longer alkyl chains i.e. $[Zn(S_2CO^nPen)_2]$ (**17**), $[Zn(S_2CO^nHex)_2]$ (**18**), $[Zn(S_2CO^nHep)_2]$ (**19**) or $[Zn(S_2CO^nOct)_2]$ (**20**) tends to consist of three steps, because as the chains grow longer, the organic side products from decomposition may have higher boiling points and are not lost as easily. In all cases, the experimental residual mass was approximately equal to the theoretical residual mass of ZnS material, which demonstrates that the decomposition in all cases is relatively clean and potentially free of significant organic contamination.

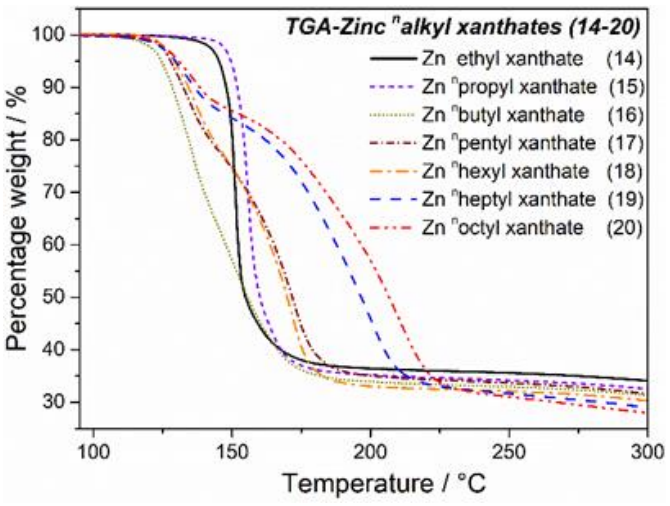

Figure 8 Thermogravimetric analysis (TGA) curves of bis(O-alkylxanthato)zinc(II), complexes **14**–**20**; heated in the range 100 – 300 °C with a temperature gradient of 10.0 °C min^{-1}.

It is known that metal xanthate complexes decompose to metal sulfides via Chugaev elimination.[1,33] Initially this proceeds by skeletal rearrangement of the ligand, hence the ligand structure can dictate the thermal profile observed and the structure of ligand is therefore the predominant factor to determine the onset temperature of decomposition.[40] The metal entity does not appear to affect the reaction pathway overlap to a large extent (iron being a major exception).[33] Having synthesized a family of both Cd and Zn xathates we decided to investigate this phenomenon. The endothermic decomposition as a function of temperatures changes in heat capacity were determined using differential scanning calorimetry (DSC). Figure 9 shows the approximately linear correlation between alkyl hydrocarbon chain length and the energy required for decomposition for bis(O-alkylxanthato)cadmium(II), complexes (**7**–**13**) and bis(O-alkylxanthato)zinc(II), complexes (**14**–**20**). The calorimetric enthalpies (ΔH_{ca}) of the phase transition was expressed by multiplying the integrated peaks by calorimetric constant.[36] it may be concluded from this data that alky chain length increases in general the energy required to initiate decomposition is increased in Cd and Zn xanthate complexes. It has been reported,[34-38] that as the chain length increases, the enthalpy of fusion is decreases and the enthalpy of exothermic decomposition increases. For Cd complexes specifically this is associated with the larger enthalpy of formation of the metal xanthato moiety at longer hydrocarbon chains.[20,39]

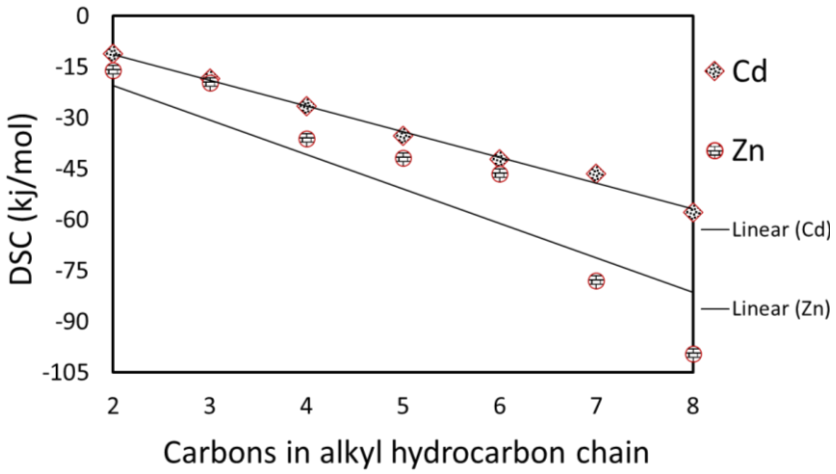

Figure 9 Showing an approximately linear correlation between number of carbons in the alkyl hydrocarbon chain of xanthate ligands and the energy required for decomposition from differential scanning calorimetry (DSC) for bis(O-alkylxanthato)cadmium(II) complexes (**7**–**13**); and bis(O-alkylxanthato)zinc(II) complexes (**14**–**20**); the samples were heated from ambient temperature to 600 °C, at rate of 10.0 °C min^{-1}.

Table 1 Thermal data for bis(O-alkylxanthato) zinc(II) compounds **14**–**20**.

SSPs	Alkyl C-chain	Decomposition steps	Experimental Residual mass (%)	Theoretical Residual mass (final step) (%)	Measured melting point (°C)	Calculated melting point (onset) (°C)
(**14**)	C_2	Initial	99.16	31.67	140–142	143.1
		2^{nd}	35.24			
(**15**)	C_3	Initial	99.5	29.02	139–141	142.3
		2^{nd}	33.77			
(**16**)	C_4	Initial	99.48	26.78	128–130	128
		2^{nd}	32.42			
(**17**)	C_5	Initial	99.64	24.86	126–128	128.5
		2^{nd}	77.26			
		3^{rd}	31.15			
(**18**)	C_6	Initial	99.8	23.20	128–130	130.4
		2^{nd}	73.34			
		3^{rd}	29.5			
(**19**)	C_7	Initial	99.48	21.74	124–126	125
		2^{nd}	82.77			
		3^{rd}	28.5			
(**20**)	C_8	Initial	99.76	20.46	123–125	122.1
		2^{nd}	83.57			
		3^{rd}	27.4			

Synthesis and Structural Characterization of CdS and ZnS Thin Films

Deposition of typical thin films on glass was achieved by spin-coating metal sulfide precursors (**7**–**20**) dissolved in tetrahydrofuran (THF) solvent on glass substrates. Films of the precursors were then annealed at different growth temperatures, 300 or 200 °C, in a furnace tube under dinitrogen N_2 flow for 60 min to furnish the metal chalcogenide thin films. The resulting thin films of cadmium or zinc sulfides were uniform and yellow or black in colour.

To confirm that CdS films were successfully formed by the thermal decomposition of bis(alkylxanthato)cadmium(II) complexes, thin films from spin coating were subjected to X-ray powder diffraction (pXRD). The diffraction patterns of films prepared from a tetrahydrofuran solution of [Cd($S_2CO^nEt)_2$] (**7**), [Cd($S_2CO^nPr)_2$] (**8**), [Cd($S_2CO^nBu)_2$] (**9**), [Cd($S_2CO^nPen)_2$] (**10**), [Cd($S_2CO^nHex)_2$] (**11**), [Cd($S_2CO^nHep)_2$] (**12**) or [Cd($S_2CO^nOct)_2$] (**13**) (labelled as ^{C2}Cd–^{C8}Cd for complexes **7**–**13**, respectively in Figure 10) and annealed at temperatures 300 °C for 60 min were recorded. Figure 10 shows the pXRD patterns of the nanocrystalline CdS thin films obtained (^{C2}Cd–^{C8}Cd). The diffraction peaks were indexed to the (100), (002), (101), (102), (110), (103), (112), (203), (211) and (105) planes of hexagonal CdS (a = 4.14 Å, and b = 6.72 Å; ICDD no: 00-041-1049). Generally, peaks grow sharper as the annealing temperature increases, which we attribute to a decrease in Scherrer broadening indicating that the size of the crystalline domains in thin films increases as synthesis temperature increases.[4] The p-XRD patterns of all films deposited at 300 °C from a THF solution of precursors **7**-**13** show a similar trend. The p-XRD pattern of films [Cd($S_2COPr)_2$] (**8**) and [Cd($S_2CO^nOct)_2$] (**13**) at 300 °C can be indexed to hexagonal CdS (Figure 11). The lattice parameters of hexagonal structure for films ^{C2}Cd–^{C8}Cd are shown in ESI; Table S9. Energy-dispersive X-ray spectroscopy (EDS) of cadmium sulfide films showed an approximately 1:1 ratio of Cd:S, the results were shown in ESI; Table S10. The chemical composition and elementals ratios by X-ray photoelectron spectroscopy XPS binding energy were shown in ESI; Table S11 and Figure S32. The atomic ratio of CdS that analysed by EDS was approximately 1.00 ± 0.06, while the atomic ratio of Cd:S analysed by XPS was also approximately 1.00 ± 0.08.

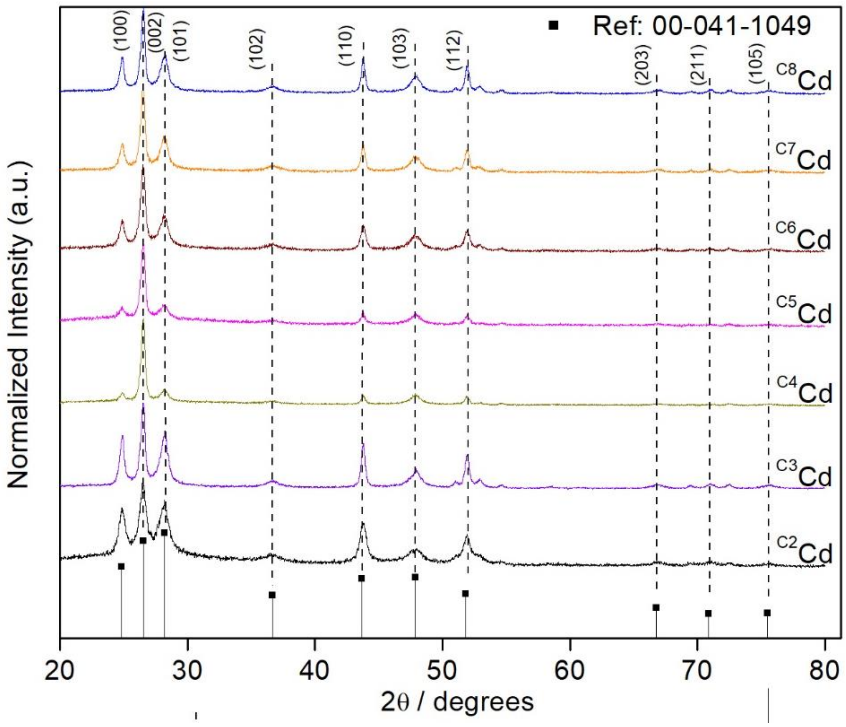

Figure 10 Grazing incidence X-ray diffraction (GIXRD) patterns of cadmium sulfide thin films (^{C2}Cd–^{C8}Cd) from the series of bis(O-alkylxanthato)cadmium(II), precursors (**7**–**13**) by a spin-coating method and annealing at 300 °C under dinitrogen N_2 for 60 min.

Powder-XRD patterns of zinc sulfide films (^{C2}Zn–^{C8}Zn) prepared from a tetrahydrofuran solution of [Zn($S_2CO^nEt)_2$] (**14**), [Zn($S_2CO^nPr)_2$] (**15**), [Zn($S_2CO^nBu)_2$] (**16**), [Zn($S_2CO^nPen)_2$] (**17**), [Zn($S_2CO^nHex)_2$] (**18**), [Zn($S_2CO^nHep)_2$] (**19**) or [Zn($S_2CO^nOct)_2$] (**20**) by spin-coating on a glass substrate and annealing at 200 °C for 60 m. under dinitrogen N_2, (Figure S33) The diffraction patterns of thin films corresponded to zinc blende (cubic ZnS, ICDD no, 00-0005-0566). The chemical compositions and elemental ratios of ZnS films by EDS measurements were recorded for ^{C4}Zn, ^{C6}Zn and ^{C8}Zn (See Table S10). The atomic ratio of Zn:S in most cases was close to 1.00 which suggests the formation of stoichiometric zinc sulfide.

The particle size and distribution of CdS films derived from the spin coating and annealing at 300 °C of precursors **9–11** and **13** were studied using HRTEM. The TEM images of films from thermal decomposition of [Cd($S_2CO^nBu)_2$] (**9**), [Cd($S_2CO^nPen)_2$] (**10**), [Cd($S_2CO^nHex)_2$] (**11**), and [Cd($S_2CO^nOct)_2$] (**13**) are shown in Figure 12 (a–d), respectively. Figure 12 (d), shows the selected area electron diffraction (SAED) pattern, high-resolution TEM image with the fast Fourier

transformation (FFT) pattern and the particles' size distribution, the moiré fringes of two overlapping crystal lattices is imaged in Figs 11 (c) and (d).[41] The SAED pattern is hexagonal and shows the (100) and (101) planes. This is consistent with p-XRD results, which indicate that the product is hexagonal CdS.[1]

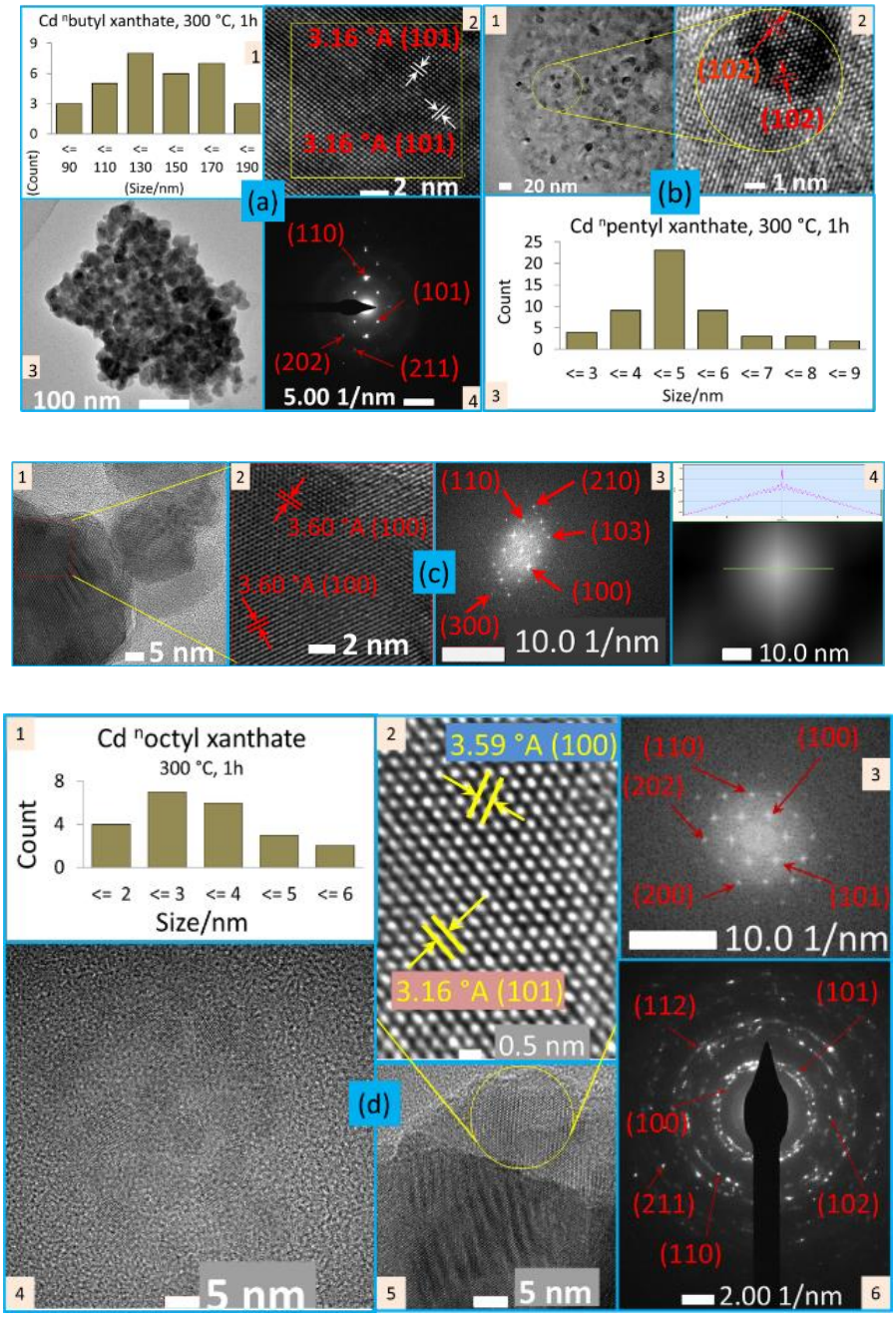

Figure 11 Characterisation of CdS crystallites taken from thin films produced at 300 °C for 60 min from [$Cd(S_2COR)_2$], precursors (**9**–**11**) and **13** by TEM. (a1–4) TEM images of ^{C4}Cd film; (b1–4) TEM images of ^{C5}Cd film; (c1–4) TEM images of ^{C6}Cd film; and (d1–6) TEM images of cadmium sulfide ^{C8}Cd film shows, (d1) particle size distribution; (d2) HRTEM image; (d3) FFT obtained from the area in panel (d6); (d4) CTEM image; (d5) structure morphology; and (d6) planes rings corresponding to SAED pattern with indexing, obtained from the area in panel (d2) that highlighted by a yellow circle in panel (d5).

In Figure 12 (e–g), TEM images of zinc sulfide crystallites from thin films that were produced by decomposition of [$Zn(S_2CO^nBu)_2$] (**16**); [$Zn(S_2CO^nHex)_2$] (**18**); and [$Zn(S_2CO^nOct)_2$] (**20**) at 200 °C are shown. HRTEM images, fast Fourier transformation FFT and selected area electron diffraction SAED patterns demonstrate the crystallinity of the films. Figure 13 (g) shows crystallites from the zinc sulfide film derived from [$Zn(S_2CO^nOct)_2$] (**20**) have wave-like fringes, inside and around the green border as reported by Lackner.[44] Pradhan et al., previously described these as important features in the transition from nano-rod to nanowire during crystal growth.[45]

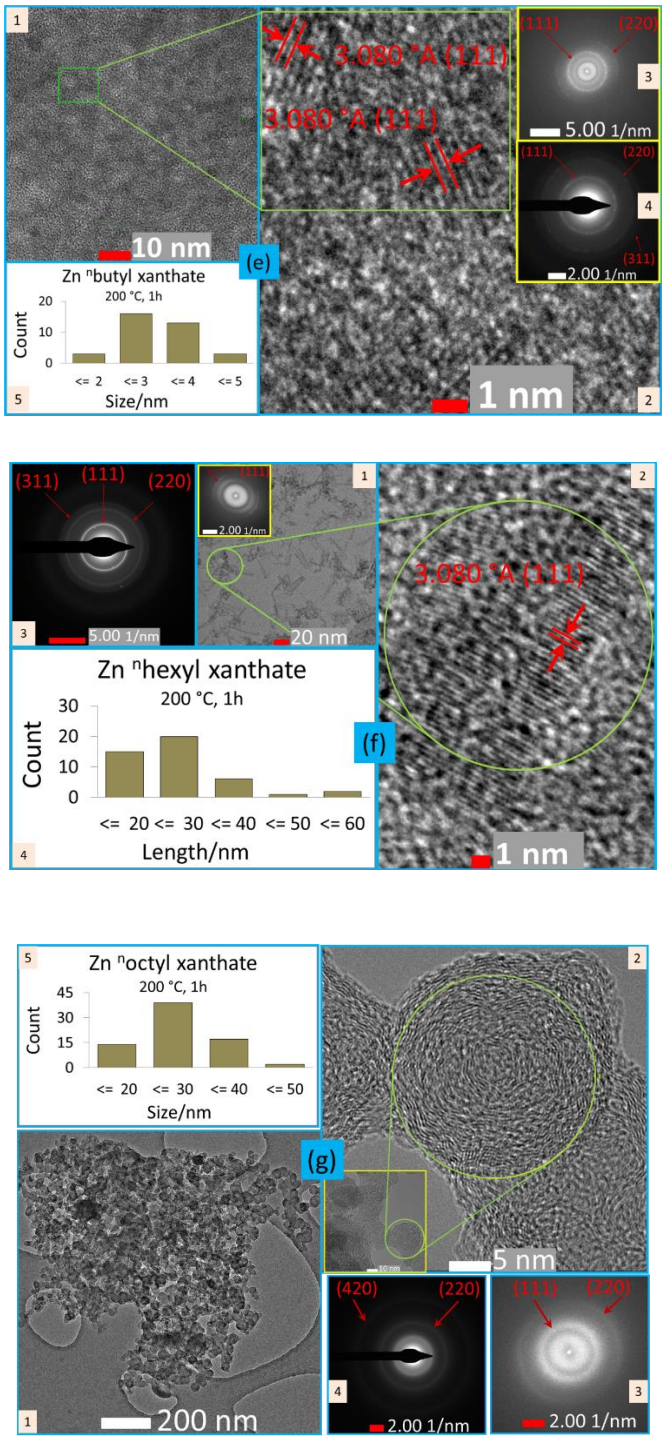

Figure 12 TEM characterization of crystallites from ZnS films produced at 200 °C for 60 min from [$Zn(S_2COR)_2$], precursors **16**, **18** and **20**. (e1-5) TEM images of ^{C4}Zn film; and (f1–4) TEM images of ^{C6}Zn film; both films include SAED pattern with indexing, FFT, HRTEM image,

structural morphology, and the histogram of particle length. (g1–5) TEM images of zinc sulfide ^{C8}Zn film shows, (g1) conventional transmission electron microscope CTEM image; (g2) HRTEM image, the inset image is the structural morphology of the selected area at 10 nm magnification scale; (g3) FFT of HRTEM image of panel (g2) with the plane indexing; (g4) planes rings corresponding to SAED pattern with indexing, obtained from the highlighted area by a green circle in panel (g2); and (g5) the histogram of particles size distribution.

Photophysical Characterisation of CdS Thin Films

Absorption spectroscopy was carried out after the films were deposited on to a glass substrate with each of the resulting spectra (See Figure S34) showing an absorption onset between 580 nm and 600 nm. The optical band-gap, E_g, for each film was determined via a Tauc plot (See Figure S34). This analysis yielded band gap energies (E_g) in the range 2.25–2.43 eV (See Table S12), consistent with a previous report using metal xanthate complexes to produce CdS.[1]

Photoluminescence (PL) spectra are shown in Figure S35 for ^{C2}Cd–^{C8}Cd films produced by spin-coating the complexes (**7**–**13**) and annealing at 300 °C. Thin films ^{C2}Cd–^{C8}Cd were dispersed prior to the measurement in N-methyl-2-pyrrolidone (NMP) solvent. In each case, a broad PL band spanning the visible spectrum is observed, on top of which are superimposed a number of peaks. In particular, peaks in the emission spectra are observed at 2.35 eV (527 nm) and 2.2 eV (564.5 nm), which are attributed to a transition across the band-gap, broadly consistent with the E_g values determined above, and a transition from a band edge to a defect state, respectively. have reported the luminescence properties of CdS thin films produced at different temperatures, and found that the spectral features of the films depend on the annealing temperature post-deposition. For annealing at 300 °C, the observed PL had a peak at 527 nm, consistent with ^{C2}Cd–^{C8}Cd films (See Figure S35). Mlowe et al. also reported the features of PL spectra for CdS films, and for an excitation wavelength of 350 nm observed broad emission in the 450–600 nm range and with a peak at a similar wavelength of 515 nm.[42] Photoluminescence decay transients for the ^{C2}Cd–^{C8}Cd films are shown in Figure 13. All decays can be fitted by a tri-exponential decay function (See Equation S1). The parameter values resulting from this fitting are given in the ESI (Figure S36 and accompanying text). The decay is almost identical in all cases and can be described by a

triexponential function comprised of three components with fitted decays ~0.15 ns, ~2 ns and ~9 ns. The first of these corresponds to the instrument response function of the system. We attribute the short component of 2 ns to non-radiative recombination due to defects in the films, whilst the longer component of 9 ns is ascribed to radiative recombination.[43]

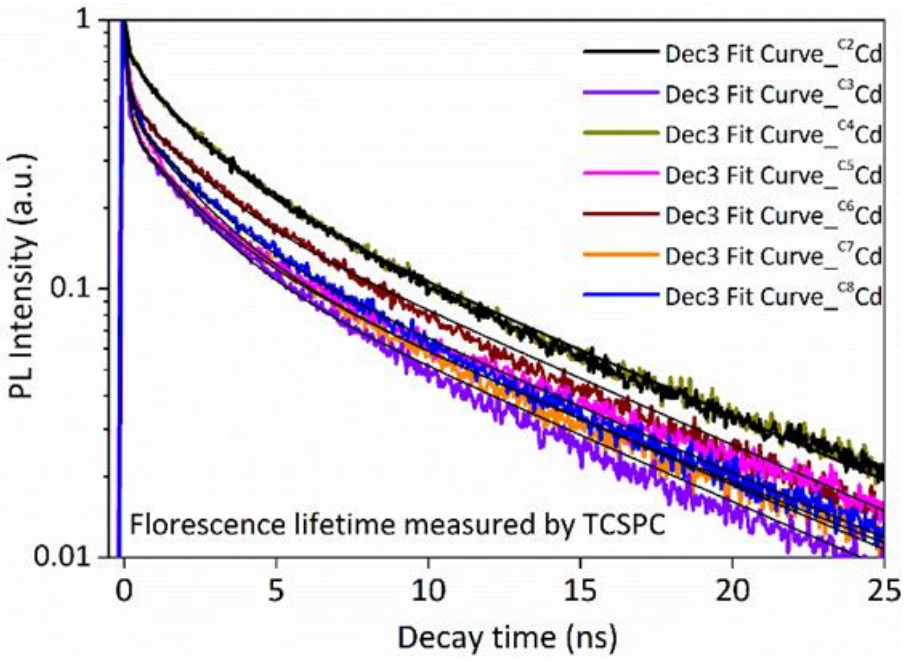

Figure 13 PL decay transients of the ^{C2}Cd–^{C8}Cd films for an excitation wavelength of λ_{ex} = 420 nm and an emission wavelength λ_{em} of 530 nm.

Conclusions

In summary, this study describes the synthesis and properties of a series of Cd(II) and Zn(II) complexes, and explores the relationship between precursor structure and resulting thin film metal sulfide. The precursors were recrystallized, single crystals were fully characterized and compounds were used to prepared CdS and ZnS semiconductor films by spin coating and thermal decomposition. An analytical study of the films consequent the thermal decomposition was carried out.

The cadmium or zinc bis(alkylxanthato) compounds [M($S_2CO^nEt)_2$] (**7** or **14**), [M($S_2CO^nPr)_2$] (**8** or **15**), [M($S_2CO^nBu)_2$] (**9** or **16**), [M($S_2CO^nPen)_2$] (**10** or **17**), [M($S_2CO^nHex)_2$] (**11** or **18**),

[$M(S_2CO^nHep)_2$] (**12** or **19**) or [$M(S_2CO^nOct)_2$] (**13** or **20**) have been successfully characterized.The X-ray structures of crystals [$Cd(S_2CO^nPr)_2$] (**8**), [$Cd(S_2CO^nBu)_2$] (**9**), [$Cd(S_2CO^nPen)_2$] (**10**), [$Cd(S_2CO^nHex)_2$] (**11**), [$Cd(S_2CO^nHep)_2$] (**12**), [$Cd(S_2CO^nOct)_2$] (**13**), [$Zn(S_2CO^nHex)_2$] (**18**) and [$Zn(S_2CO^nHep)_2$] (**19**), have been reported. We show that there is an approximately linear relationship between the alkyl chain length in these complexes and the energy required for decomposition to the corresponding crystalline metal sulfide i.e. CdS or ZnS. Spin coating of these precursors followed by a thermal annealing step was therefore used to produce thin films of cadmium or zinc sulfide at temperatures as low as 200 °C. Overall, the spin coating/annealing method is a promising of producing transition metal sulfide films at a relatively low temperatures.

Supporting information

Supporting information is available online at the ACS website.

Acknowledgements

This work was supported by the Ministry of Higher Education and Scientific Research of Iraq 'MOHESR-IQ' and the University of Babylon, Iraq. AAKB thanks Maria A. Leontiadou, Department of Physics and Astronomy and Photon Science Institute for useful discussions regarding steady-state PL and TCSPC experiments.

Author Affiliations

[a] Dept. of Materials, University of Manchester, Oxford Road, Manchester M13 9PL, UK
[b] Dept. of Chemistry, University of Manchester, Oxford Road, Manchester M13 9PL, UK
[c] Dept. of Physics and Astronomy and Photon Science Inst., University of Manchester, M13 9PL, UK

Corresponding Author

*David J. Lewis, University of Manchester, Department of Materials email: david.lewis-4@manchester.ac.uk

References

(1) Bakly, A. A.; Spencer, B. F.; O'Brien, P. The Deposition of Thin Films of Cadmium Zinc Sulfide Cd1−x Zn x S at 250 °C from Spin-Coated Xanthato Complexes: A Potential Route to Window Layers for Photovoltaic Cells. *J. Mater. Sci.* **2017**, *53* (6), 4360–4370. https://doi.org/10.1007/s10853-017-1872-1.

(2) Ramasamy, K.; Malik, M. A.; O'Brien, P.; Raftery, J. ZnS, CdS and ZnxCd1-XS Thin Films from Zn (II) and Cd (II) Complexes of 1, 1, 5, 5-Tetramethyl-2-4-Dithiobiuret As Single Molecular Precursors. *Mater. Res. Soc Proc* **2008**, *4*, 1145–1151.

(3) Ramasamy, K.; Malik, M. A.; O'Brien, P.; Raftery, J. Metal Complexes of Thiobiurets and Dithiobiurets: Novel Single Source Precursors for Metal Sulfide Thin Film Nanostructures. *Dalt. Trans.* **2010**, *39*, 1460–1463. https://doi.org/10.1039/B923179J.

(4) Nair, P. S.; Radhakrishnan, T.; Revaprasadu, N.; Kolawole, G.; O'Brien, P. Cadmium Ethylxanthate: A Novel Single-Source Precursor for the Preparation of CdS Nanoparticles. *J. Mater. Chem.* **2002**, *12*, 2722–2725. https://doi.org/10.1039/b202072f.

(5) Zhang, W. M.; Sun, Z. X.; Hao, W.; Su, D. W.; Vaughan, D. J. Synthesis of Size Tuneable Cadmium Sulphide Nanoparticles from a Single Source Precursor Using Ammonia as the Solvent. *Mater. Res. Bull.* **2011**, *46* (12), 2266–2270. https://doi.org/10.1016/j.materresbull.2011.08.062.

(6) Pradhan, N.; Katz, B.; Efrima, S. Synthesis of High-Quality Metal Sulfide Nanoparticles from Alkyl Xanthate Single Precursors in Alkylamine Solvents. *J. Phys. Chem. B* **2003**, *107* (50), 13843–13854. https://doi.org/10.1021/jp035795l.

(7) Mietlarek-Kropidłowska, A.; Chojnacki, J.; Strankowski, M.; Fahmi, A.; Gazda, M.; Becker, B. Cadmium Complex Possessing Simultaneously Silanethiolato- and Dithiocarbamato-Ligands. A Novel Single-Source Precursor of Cadmium Sulfide. *J. Therm. Anal. Calorim.* **2014**, *118* (2), 993–1001. https://doi.org/10.1007/s10973-014-3842-z.

(8) Britt, J.; Ferekides, C. Thin-Film CdS/CdTe Solar Cell with 15.8% Efficiency. *Appl. Phys.*

Lett. **1993**, *62* (22), 2851–2852.

(9) Wang, X.; Zhuang, J.; Peng, Q.; Li, Y. A General Strategy for Nanocrystal Synthesis. *Nature* **2005**, *437* (7055), 121–124. https://doi.org/0.1038/nature03968.

(10) Ma, C.; Moore, D.; Ding, Y.; Li, J.; Wang, Z. L. Nanobelt and Nanosaw Structures of II-VI Semiconductors. *Int. J. Nanotechnol.* **2004**, *1* (4), 431–451.

(11) Moore, D.; Wang, Z. L. Growth of Anisotropic One-Dimensional ZnS Nanostructures. *J. Mater. Chem.* **2006**, *16* (40), 3898–3905.

(12) Abrahams, B. F.; Hoskins, B. F.; Tiekink, E. R. T.; Winter, G. Investigation of a New Xanthate Ligand. The Crystal and Molecular Structures of Nickel and Cadmium (Methoxyethyl) Xanthates. *Aust. J. Chem.* **1988**, *41* (7), 1117–1122.

(13) Thomas, P. J.; Stansfield, G. L.; Komba, N.; Cant, D. J. H.; Ramasamy, K.; Albrasi, E.; Al-Chaghouri, H.; Syres, K. L.; O'Brien, P.; Flavell, W. R.; Mubofu, E.; Bondino, F.; Magnano, E. Growth of Nanocrystalline Thin Films of Metal Sulfides [CdS, ZnS, CuS and PbS] at the Water-Oil Interface. *RSC Adv.* **2015**, *5*, 62291–62299. https://doi.org/10.1039/C5RA09417H.

(14) Lewis, E.; Haigh, S.; O'Brien, P. The Synthesis of Metallic and Semiconducting Nanoparticles from Reactive Melts of Precursors. *J. Mater. Chem. A* **2014**, *2* (3), 570–580. https://doi.org/10.1039/C3TA12900D.

(15) Afzaal, M.; Malik, M. A.; O'Brien, P. Chemical Routes to Chalcogenide Materials as Thin Films or Particles with Critical Dimensions with the Order of Nanometres. *J. Mater. Chem.* **2010**, *20*, 4031–4040. https://doi.org/10.1039/B923898K.

(16) Ramasamy, K.; Malik, M. A.; Revaprasadu, N.; O'Brien, P. Routes to Nanostructured Inorganic Materials with Potential for Solar Energy Applications. *Chem. Mater.* **2013**, *25*, 3551–3569. https://doi.org/10.1021/cm401366q.

(17) Dance, I. G. The Structural Chemistry of Metal Thiolate Complexes. *Polyhedron* **1986**, *5* (5), 1037–1104.

(18) Matthews, P. D.; McNaughter, P. D.; Lewis, D. J.; O'Brien, P. Shining a Light on Transition Metal Chalcogenides for Sustainable Photovoltaics. *Chem. Sci.* **2017**, *8*, 4177–4187.

(19) Ramasamy, K.; Malik, M. A.; Helliwell, M.; Raftery, J.; O'Brien, P. Thio-and Dithio-Biuret Precursors for Zinc Sulfide, Cadmium Sulfide, and Zinc Cadmium Sulfide Thin Films. *Chem. Mater.* **2011**, *23*, 1471–1481.

(20) McNaughter, P. D.; Saah, S. A.; Akhtar, M.; Abdulwahab, K.; Malik, M. A.; Raftery, J.; Awudza, J. A. M.; O'Brien, P. The Effect of Alkyl Chain Length on the Structure of Lead(II) Xanthates and Their Decomposition to PbS in Melt Reactions. *Dalton Trans.* **2016**, *45*, 16345–16353.

(21) MacLachlan, A. J.; Rath, T.; Cappel, U. B.; Dowland, S. A.; Amenitsch, H.; Knall, A. C.; Buchmaier, C.; Trimmel, G.; Nelson, J.; Haque, S. A. Polymer/Nanocrystal Hybrid Solar Cells: Influence of Molecular Precursor Design on Film Nanomorphology, Charge Generation and Device Performance. *Adv. Funct. Mater.* **2015**, *25* (3), 409–420. https://doi.org/10.1002/adfm.201403108.

(22) Lewis, E. A.; McNaughter, P. D.; Yin, Z.; Chen, Y.; Brent, J. R.; Saah, S. A.; Raftery, J.; Awudza, J. A. M.; Malik, M. A.; O'Brien, P. In Situ Synthesis of PbS Nanocrystals in Polymer Thin Films from Lead (II) Xanthate and Dithiocarbamate Complexes: Evidence for Size and Morphology Control. *Chem. Mater.* **2015**, *27*, 2127–2136.

(23) Abdelhady, A. L.; Malik, M. A.; O'Brien, P. Colloidal Synthesis of ZnS, CdS and ZnxCd12xS Nanoparticles from Zinc and Cadmium Thiobiuret Complexes. *J. Inorg. Organomet. Polym. Mater.* **2014**, *24* (1), 226–240.

(24) Ouachtari, F. Influence of Bath Temperature, Deposition Time and S/Cd Ratio on the Structure, Surface Morphology, Chemical Composition and Optical Properties of CdS Thin Films Elaborated by Chemical Bath Deposition. *J. Mod. Phys.* **2011**, *02*, 1073–1082. https://doi.org/10.4236/jmp.2011.29131.

(25) Bondi, A. Van Der Waals Volumes and Radii. *J. Phys. Chem.* **1964**, *68* (3), 441–451.

(26) Tiekink, E. R. T.; Haiduc, I. Stereochemical Aspects of Metal Xanthate Complexes:

Molecular Structures and Supramolecular Self-Assembly. *Prog. Inorg. Chem.* **2005**, *54*, 127–319.

(27) Iimura, Y.; Ito, T.; Hagihara, H. The Crystal Structure of Cadmium Ethylxanthate. *Acta Crystallogr. Sect. B Struct. Crystallogr. Cryst. Chem.* **1972**, *28* (7), 2271–2279. https://doi.org/10.1107/S0567740872005904.

(28) Rietveld, H. M.; Maslen, E. N. The Crystal Structure of Cadmium N-Butyl Xanthate. *Acta Crystallogr.* **1965**, *18* (3), 429–436. https://doi.org/10.1107/S0365110X65000956.

(29) Harcourt, R. D.; Winter, G. The Asymmetric M-S Bonds in Metal Xanthates. *J. Inorg. Nucl. Chem.* **1975**, *37* (4), 1039–1041.

(30) Tiekink, E. R. T. Molecular Architecture and Supramolecular Association in the Zinc-Triad 1, 1-Dithiolates. Steric Control as a Design Element in Crystal Engineering? *CrystEngComm* **2003**, *5* (21), 101–113.

(31) Lai, C. S.; Lim, Y. X.; Yap, T. C.; Tiekink, E. R. T. Molecular Paving with Zinc Thiolates. *CrystEngComm* **2002**, *4* (99), 596–600.

(32) Ito, T. The Crystal Structure of Zinc Isopropylxanthate. *Acta Crystallogr. Sect. B Struct. Crystallogr. Cryst. Chem.* **1972**, *28* (6), 1697–1704.

(33) Piquette, A. Fabrication of Nanometric Metal Sulfides from Xanthate Precursors, Oklahoma State University, 2007.

(34) Mackenzie, R. C.; Mitchell, B. D. Differential Thermal Analysis. A Review. *Analyst* **1962**, *87* (1035), 420–434.

(35) Watson, E. S.; O'neill, M. J.; Justin, J.; Brenner, N. A Differential Scanning Calorimeter for Quantitative Differential Thermal Analysis. *Anal. Chem.* **1964**, *36* (7), 1233–1238.

(36) Cooper, A.; Nutley, M. A.; Wadood, A. Differential Scanning Microcalorimetry. *Protein-ligand interactions: Hydrodynamics and calorimetry*. Oxford University Press, Oxford, NY 2000, pp 287–318.

(37) John, G. T.; Alexander, L. T. Thermal Study of Some Metal Ethyl Xanthates. *Int. J. Appl.*

2014, *4* (2), 218–223.

(38) Coats, A. W.; Redfern, J. P. Thermogravimetric Analysis. A Review. *Analyst* **1963**, *88* (1053), 906–924.

(39) Shen, Y. Chemical Fate Studies of Mining Reagents: Understanding the Decomposition Behavior under Various Conditions, Columbia University, 2016.

(40) Heuer-Jungemann, A.; Feliu, N.; Bakaimi, I.; Hamaly, M.; Alkilany, A.; Chakraborty, I.; Masood, A.; Casula, M. F.; Kostopoulou, A.; Oh, E. et al. The Role of Ligands in the Chemical Synthesis and Applications of Inorganic Nanoparticles. *Chem. Rev.* **2019**, *119* (8), 4819–4880.

(41) Majumder, M.; Chakraborty, A. K.; Mallik, B. Photoluminescence Studies on Nanostructured Cadmium Sulfide Thin Films Prepared by Chemical Bath Deposition Method and Annealed at Different Temperatures. *J. Lumin.* **2010**, *130* (8), 1497–1503.

(42) Mlowe, S.; Lewis, D. J.; Malik, M. A.; Raftery, J.; Mubofu, E. B.; O'Brien, P.; Revaprasadu, N. Bis (Piperidinedithiocarbamato) Pyridinecadmium (II) as a Single-Source Precursor for the Synthesis of CdS Nanoparticles and Aerosol-Assisted Chemical Vapour Deposition (AACVD) of CdS Thin Films. *New J. Chem.* **2014**, *38* (12), 6073–6080.

(43) Bawendi, M. G.; Carroll, P. J.; Wilson, W. L.; Brus, L. E. Luminescence Properties of CdSe Quantum Crystallites: Resonance between Interior and Surface Localized States. *J. Chem. Phys.* **1992**, *96* (2), 946–954.

(44) Lackner, M. *Combustion Synthesis: Novel Routes to Novel Materials*; Bentham Science Publishers, 2010.

(45) Pradhan, N.; Efrima, S. Supercrystals of Uniform Nanorods and Nanowires, and the Nanorod-to-Nanowire Oriented Transition. *J. Phys. Chem. B* **2004**, *108* (32), 11964–11970.

Table of Contents Graphic [FOR TABLE OF CONTENTS ONLY]

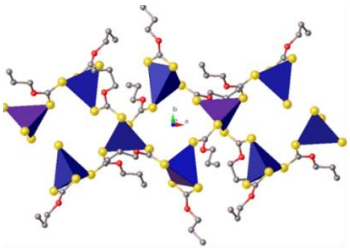

SYNOPSIS [For Table of contents only]: Bakly et al investigate tuning of the molecular structure of a series of O-alkylxanthato zinc and cadmium precursor complexes for the production of ZnS and CdS materials.